# Giant Rashba-type splitting in molybdenum-driven bands of $MoS_2$/Bi(111) heterostructure

Kyuhwan Lee,* Won Seok Yun,* and J. D. Lee†
*Department of Emerging Materials Science, DGIST, Daegu 711-873, Republic of Korea*
(Received 21 November 2014; revised manuscript received 2 March 2015; published 16 March 2015)

We investigate the electronic band structure of the $MoS_2$/Bi(111) heterostructure, for which the supercell calculation is performed due to the lattice mismatch between two structures but the effective primitive cell is recovered by using the band unfolding technique. It is found that the strong molybdenum-bismuth band hybridization together with a generation of the interfacial dipole field induces the giant Rashba-type splitting accompanying the proper spin topology in molybdenum-driven bands at the Γ point. Similar splittings are also found in the heterostructure with other transition-metal dichalcogenides, i.e., with $MoSe_2$, $WS_2$, and $WSe_2$.

DOI: 10.1103/PhysRevB.91.125420 PACS number(s): 71.15.Mb, 71.70.Ej, 75.70.Cn, 71.20.Mq

## I. INTRODUCTION

Two-dimensional (2D) semiconducting materials have attracted intensive attention due to their various potential applications in nanoscale electronics, photonics, valleytronics, spintronics, and so on [1–8]. In particular, molybdenum disulfide ($MoS_2$), a representative of the transition-metal dichalcogenides (TMDCs), is known to have unique electronic properties, showing a strong dependence on the layer thickness and the mechanical strain [2,9]. Recently, there has been a growing interest in the hybrid systems of $MoS_2$ with other 2D architectured materials in order to explore an abundance of the electronic properties. For instance, the $MoS_2$/graphene heterostructure is reported to show a high electronic conductivity and other outstanding electrochemical or thermoelectric properties [10,11].

Bismuth (Bi) also attracts a great deal of attention for another reason. Bi is a main building block for the topological insulator (TI), a new insulating phase in the solid state. In particular, 2D ultrathin Bi(111) films were theoretically predicted to be elemental 2D TI materials [12–14] and experimentally synthesized and characterized [15,16]. A physical origin for such elemental TI properties resides in a remarkable feature of Bi that it is one of the main group elements that has the strongest spin-orbit coupling (SOC). Bulk Bi has a bilayered structure with an $ABC$ stacking sequence along the (111) direction. Within a puckered bilayer (BL) where atoms form a hexagonal lattice, an atom is covalently bonded to its three nearest neighbors. Its next-nearest neighbors are in the adjacent BLs.

Rashba spin splitting [17] of electronic bands in the surface or interface provides a new chance for the spintronic device application without the magnetic field, for instance, the spin field-effect transistor (FET) [18]. It is driven by the inversion symmetry breaking via SOC, which leads to a spin splitting in the electronic band dispersion, such as $\varepsilon_{\pm}(\mathbf{k}) = \hbar^2\mathbf{k}^2/2m^* \pm \alpha_R|\mathbf{k}|$ with $\mathbf{k} = (k_x, k_y)$. $m^*$ is the effective mass and $\alpha_R$ is the Rashba constant which determines the strength of the Rashba Hamiltonian, i.e., $\mathcal{H}_R = \alpha_R\sigma \cdot (\mathbf{k} \times \hat{\mathbf{z}})$, where $\sigma$ is the Pauli matrix vector and $\hat{\mathbf{z}}$ is the unit vector perpendicular to the plane. The spins of the electronic states $\varepsilon_{\pm}(\mathbf{k})$ are oppositely aligned within the $k_xk_y$ plane, and are normal to the wave vector $\mathbf{k}$. The effect has been observed in nonmagnetic heavy-element surfaces such as Au(111) [19,20], Ir(111) [21], Bi/Ag(111) [22], in the magnetic surface of Gd(0001) [23], or in the interface of graphene/Ni(111) [24]. This strategy may teach us an envisioning route toward a novel spintronic application of the semiconductor heterostructure.

In this paper, we investigate the electronic band structure of the $MoS_2$/BL-Bi(111) heterostructure using the first-principles calculations incorporating the state-of-the-art band unfolding technique. The effective primitive cell projected to $MoS_2$ (i.e., the $MoS_2$-projected effective band) is recovered from the supercell calculation of the heterostructure using the technique. We find the giant Rashba-type splitting in Mo-driven bands at the Γ point of the $MoS_2$/BL-Bi(111) heterostructure, accompanied by the Rashba spin topology that the spin-orbit split momentum distribution carries the antiparallel spin direction. The electronic origin is the Mo-Bi band hybridization, together with the interfacial dipole field generated in the heterostructure. Similar Rashba-type splittings are also found in TM-driven bands of other TMDC/BL-Bi(111) heterostructures, i.e., with $MoSe_2$, $WS_2$, and $WSe_2$.

## II. COMPUTATIONAL DETAILS

Calculations are performed within the framework of density functional theory (DFT) using the projector-augmented wave (PAW) method [25,26], as implemented in the Vienna Ab-initio Simulation Package (VASP) [27]. Exchange-correlation potential is treated in the generalized gradient approximation (GGA) [28], with SOC included. We use the energy cutoff of 450 eV for the plane-wave expansion on the $8 \times 8 \times 1$ $\gamma$-centered $k$-point mesh. All of the atomic positions were fully optimized using the conjugate gradient method for the geometry optimization and the van der Waals (vdW) corrected functional (optB88-vdW) [29] was employed. Owing to the lattice mismatch between two systems, we have carried out the supercell calculation with the model as illustrated in Fig. 1(e), where the $4 \times 4$ lateral periodicity of single-layer (1L) $MoS_2$ and the $3 \times 3$ lateral periodicity of BL-Bi(111) were employed, resulting in ∼3.5% lattice mismatch. An optimized lattice parameter of the interlayer spacing $\Delta d$ between 1L-$MoS_2$ and BL-Bi(111) is calculated to be 3.43 Å. The supercell calculation has a well-known longstanding difficulty leading to convoluted band structures, that is, the

*These authors contributed equally to this work.
†Corresponding author: jdlee@dgist.ac.kr

 

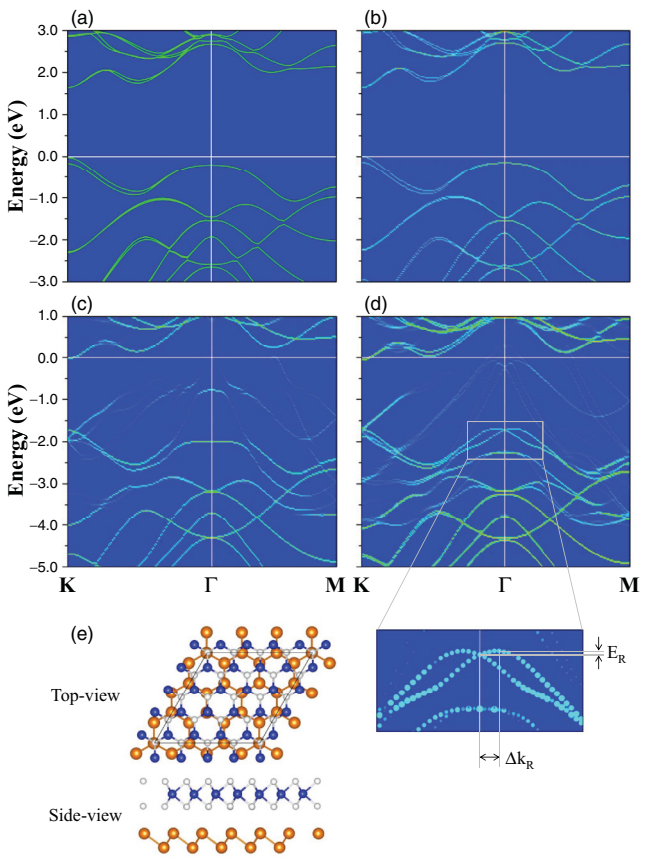


FIG. 1. (Color online) Electronic band structures of the pristine 1L-$MoS_2$ and 1L-$MoS_2$/BL-Bi(111) heterostructure. (a),(b) Band structures of the pristine 1L-$MoS_2$ from (a) the $1 \times 1$ primitive cell and (b) the $4 \times 4$ supercell incorporating the band unfolding technique. (c),(d) Electronic band structures of the 1L-$MoS_2$/BL-Bi(111) heterostructure from the $4 \times 4$ supercell (c) without SOC and (d) with SOC. Band splitting at the Γ point, denoted by the rectangular box, is zoomed. (e) Top and side views of the model of the 1L-$MoS_2$/BL-Bi(111) heterostructure. Blue and white balls stand for Mo and S atoms, respectively, and orange balls stand for Bi atoms.

zone folding of the bands. Here, we overcome this difficulty using the band unfolding technique, which employs the spinor eigenstates [30] based on the method by Popescu and Zunger [31].

## III. GIANT RASHBA-TYPE SPLITTING

### A. 1L-$MoS_2$/Bi(111) heterostructure: $MoS_2$-projected bands

We check the validity of the band unfolding technique by comparing the primitive cell calculation with the $4 \times 4$ supercell calculation for the pristine 1L-$MoS_2$. According to Figs. 1(a) and 1(b), the band structures obtained from the two calculations are almost identical. Hereafter, the electronic band structures are always obtained by the band unfolding toward the $MoS_2$-projected effective band, unless mentioned otherwise. Subsequently, the band structures of the 1L-$MoS_2$/BL-Bi(111) heterostructure without and with SOC are displayed in Figs. 1(c) and 1(b). The most dramatic effect resulting from SOC is found in the splitting of the Mo

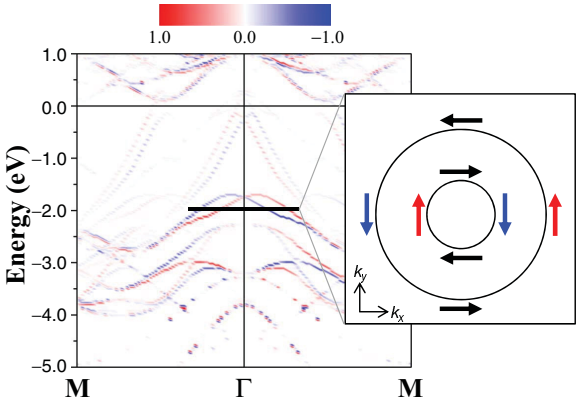


FIG. 2. (Color online) Spin-resolved electronic band structure of the 1L-$MoS_2$/BL-Bi(111) heterostructure along the highly symmetric points M-Γ-M. For the Rashba-type splitting of the Mo-driven bands at the Γ point, the spin topology in the cross section (shown in the square box) along the horizontal bar is illustrated. The red and blue colors represent two opposite spin components projected to the in-plane polarization normal to **k**.

$d_{z^2}$-dominant bands along the momentum direction at the Γ point, which is indicated by the rectangular box in Fig. 1(d). The size of the splitting is given by the momentum offset $\Delta k_R$ away from the crossing point and the corresponding energy offset $E_R$. From Fig. 1(d), we estimate $\Delta k_R$ and $E_R$ to be 0.071 $Å^{-1}$ and 37.25 meV, respectively.

The spin topology relevant in the band splitting is especially interesting. It should be remembered that the corresponding band of the pristine 1L-$MoS_2$, mostly contributed from Mo $d_{z^2}$ states [9], is spin unpolarized. Figure 2 shows, however, that the resulting spin-orbit split momentum distribution accompanies the antiparallel spin direction (see the square box in the figure), which in fact provides an evidence that the band splitting at the Γ point is the Rashba-type one. In the figure, the spin components projected to the in-plane polarization normal to **k** are indicated in two different colors [32]. From an estimation of $\Delta k_R$ and a fitting value of the effective mass ($m^* = -0.478 m_0$; $m_0$: bare electron mass), the effective Rashba constant $\alpha_R$ is obtained to be $\alpha_R = \hbar^2 \Delta k_R / m^* = 1.097$ eVÅ. This value is larger than the Au(111) surface ($\alpha_R = 0.33$ eVÅ) [19], Au/W(110) quantum well ($\alpha_R = 0.16$ eVÅ) [33], InGaAs/GaAs quantum dot ($\alpha_R \sim 0.08$–$0.12$ eVÅ) [34], or InGaAs/InAlAs heterostructure ($\alpha_R = 0.07$ eVÅ) [35], but smaller than bulk BiTeI ($\alpha_R = 3.8$ eVÅ) [36], the Bi/Ag(111) surface ($\alpha_R = 3.05$ eVÅ) [22], or a Pt-Si nanowire ($\alpha_R = 1.36$ eVÅ) [37].

In Fig. 3, a change of the Rashba-type band splitting with respect to the interlayer spacing $\Delta d$ between 1L-$MoS_2$ and BL-Bi(111) in the heterostructure is illustrated. The equilibrium value of $\Delta d$ is 3.43 Å, which actually corresponds to the band structure of Fig. 1(d). With an increase of $\Delta d$ from Figs. 3(a) to 3(c), the size of the splitting in the Mo-driven band naturally decreases. When $\Delta d$ is sufficiently large, the splitting disappears [see Fig. 3(c)]. Further insight into the relevant heterostructure is explored by manipulating the layer thickness, i.e., introducing the double layer (2L). In Figs. 4(a) and 4(b), we study the electronic structures of 2L-$MoS_2$/BL-

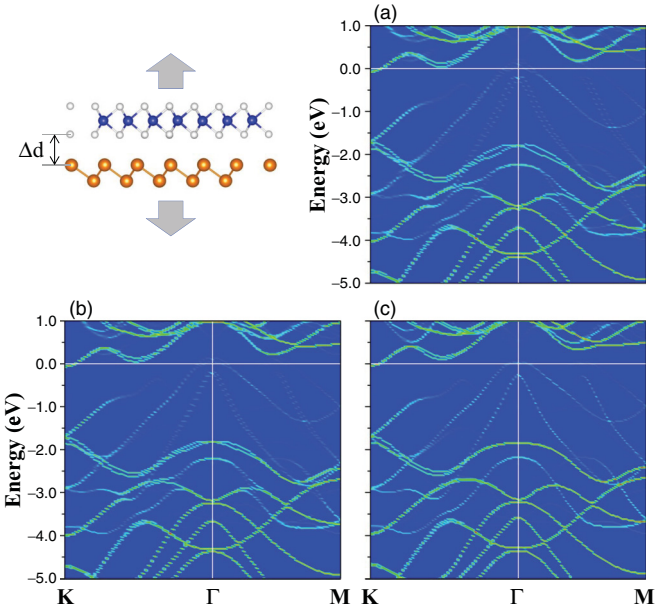


FIG. 3. (Color online) Electronic band structures of the 1L-$MoS_2$/BL-Bi(111) heterostructure system with respect to the different interlayer spacing $\Delta d$ between 1L-$MoS_2$ and BL-Bi(111), that is, an increase of $\Delta d$ from the equilibrium value (i.e., 3.43Å) (a) by ∼10%, (b) by ∼20%, or (c) by more than ∼50%.

Bi(111) and 1L-$MoS_2$/2L-BL-Bi(111) heterostructures. It is found that although the electronic band from the off-interfacial layer is bulklike, that from the interfacial layer still retains the Rashba-type splitting. This looks to be not very different between the two heterostructures.

Let us now discuss the electronic origin of the observed Rashba-type splitting. Figures 5(a) and 5(b) describe the artificially prepared systems of BL-Bi(111)/1L-$MoS_2$/BL-Bi(111) and 1L-$MoS_2$/BL-Bi(111)/1L-$MoS_2$, which have the mirror symmetry, and provide the band structures of those. In Fig. 5(a), no splitting is found in the corresponding $MoS_2$ band. This should be attributed to there being no effective dipole field on $MoS_2$ due to its cancellation in the given

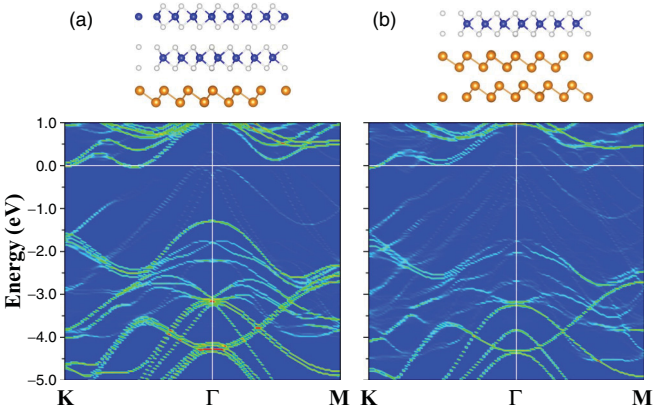


FIG. 4. (Color online) Electronic band structures of (a) 2L-$MoS_2$/BL-Bi(111) and (b) 1L-$MoS_2$/2L-BL-Bi(111) heterostructures.

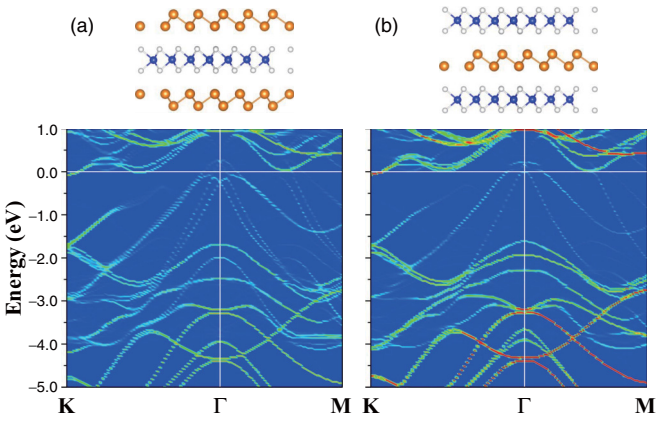


FIG. 5. (Color online) Electronic band structures of the (a) 1L-$MoS_2$/BL-Bi(111)/1L-$MoS_2$ and (b) BL-Bi(111)/1L-$MoS_2$/BL-Bi(111) heterostructures. Both of these systems are artificially prepared to have the mirror symmetry.

geometry. Meanwhile, in Fig. 5(b), although $MoS_2$ undergoes the dipole field, the Bi side (i.e., the BL-Bi assumes the inversion symmetry) cannot give the necessary hybridization. This shows that the $MoS_2$ band will not split by the dipole field alone. In contrast, in the heterostructure of Fig. 2, the characteristic spin polarization of the Mo-driven (i.e., Mo $d_{z^2}$-dominant) split band $|\psi\rangle$ suggests the strong hybridization with Bi, which will be given by

$$|\psi\rangle = |\mathrm{Mo}; d_{z^2}\rangle + c_s|\mathrm{Bi}; s\rangle + c_{p_x}|\mathrm{Bi}; p_x\rangle + c_{p_y}|\mathrm{Bi}; p_y\rangle + \cdots, \quad (1)$$

with the band coefficients $c_s$, $c_{p_x}$, $c_{p_y}$, and so on. Here, the spin-polarized Bi $s$, $p_x$, and $p_y$ orbitals, which are originated by the Rashba-type splitting in Bi under the effective dipole field, eventually determine the spin topology of the split band $|\psi\rangle$ because $|\mathrm{Mo}; d_{z^2}\rangle$ is found to have no spin polarization.

### B. 1L-TMDC/Bi(111) heterostructure: TMDC-projected bands

Trigonal-prismatic TMDCs including $MoS_2$ are quasi-2D, highly anisotropic, layered compounds and share key features of the electronic structures. Bulk TMDCs which are indirect-gap semiconductors become direct-gap semiconductors with larger gaps when the thickness reduces to a single layer [9]. Also, the Zeeman splittings at the valleys $K$ and $K'$ via SOC in bulk TMDCs ignite the valleytronic application [5–7]. In that context, it is interesting to examine the 1L-TMDC/BL-Bi(111) heterostructure. In Figs. 6(a)–6(c), the TMDC-projected effective electronic band structures of the 1L-$WS_2$/BL-Bi(111), 1L-$WSe_2$/BL-Bi(111), and 1L-$MoSe_2$/BL-Bi(111) heterostructures are provided. Rashba-type splittings at the Γ point in all three heterostructures are robust. Further, the splittings are found to be larger than the case with $MoS_2$ because W or Se are heavier atoms and generally induce stronger SOC than Mo or S [see Fig. 6(d)]. It is noted that the Rashba-type splitting can be regarded as another crucial option of 1L-TMDC for the spintronic application by forming the heterostructure with Bi.

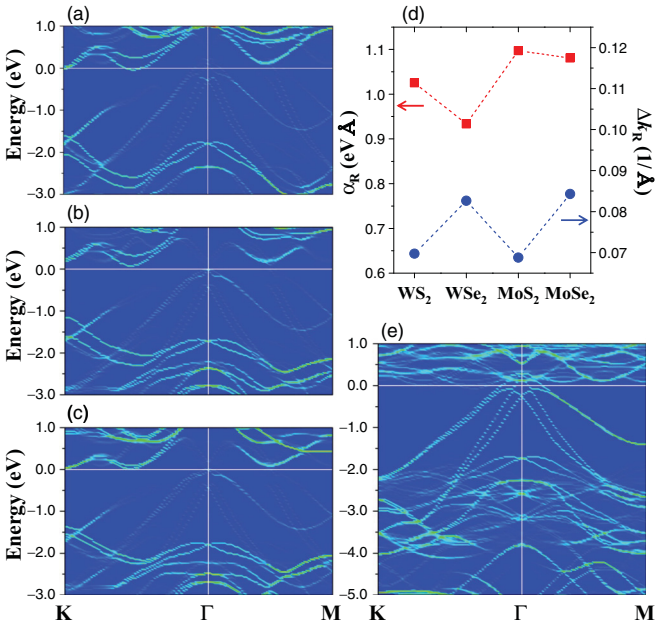


FIG. 6. (Color online) TMDC-projected effective band structures of the (a) 1L-$WS_2$/BL-Bi(111), (b) 1L-$WSe_2$/BL-Bi(111), and (c) 1L-$MoSe_2$/BL-Bi(111) heterostructures. (d) Effective Rashba constant $\alpha_R$ and band splitting parameter $\Delta k_R$ for the 1L-TMDC/BL-Bi(111) heterostructure. (e) Bi-projected effective band structure of the 1L-$MoS_2$/BL-Bi(111) heterostructure.

### C. 1L-$MoS_2$/Bi(111) heterostructure: Bi-projected bands

Figure 6(e) gives the *Bi-projected* effective band structure of the 1L-$MoS_2$/BL-Bi(111) heterostructure. Along the energy axis at the Γ point, the Rashba-type splittings in the topmost three bands ranging from near the Fermi level to ∼−2 eV are observed, which are evidently induced by the presence of 1L-$MoS_2$. In particular, the splitting near ∼−2 eV at the Γ point is almost overlapped with that of the Mo-driven bands observed in the $MoS_2$-projected effective band [see Fig. 1(d)]. This lets us indicate the merit of the band unfolding, without which the hidden splitting in the Mo-driven bands would hardly be characterized from the convoluted band structure.

## IV. SUMMARY

To summarize, we have investigated the electronic band structure of the $MoS_2$/Bi(111) heterostructure using the first-principles calculation. Due to the lattice mismatch between two materials, we carried out the supercell calculation. Instead, we recovered the effective primitive cell band adopting the state-of-the-art band unfolding method. Here we found the giant Rashba-type splitting in the molybdenum-driven bands at the Γ point of the $MoS_2$ side, whose spin topology is consistent with the Rashba spin splitting. The electronic origin is the molybdenum-bismuth band hybridization in company with the interfacial dipole field. Further, similar Rashba-type splittings are also found in other TMDC/Bi(111) heterostructures. This finding significantly widens the spintronic option of TMDC, which is known to have excellent electric properties.

## ACKNOWLEDGMENTS

We acknowledge Joongoo Kang for the encouraging discussion. This work was supported by the Leading Foreign Research Institute Recruitment Program (Grant No. 2012K1A4A3053565) and the Basic Science Research Program (Grant No. 2013R1A1A2007388) through the National Research Foundation of Korea (NRF) funded by the Ministry of Education, Science and Technology (MEST).

[1] K. S. Novoselov, D. Jiang, F. Schedin, T. Booth, V. V. Khotkevich, S. V. Morozov, and A. K. Geim, Proc. Natl. Acad. Sci. USA **102**, 10451 (2005).
[2] A. Splendiani, L. Sun, Y. Zhang, T. Li, J. Kim, C.-Y. Chim, G. Galli, and F. Wang, Nano Lett. **10**, 1271 (2010).
[3] B. Radisavljevic, A. Radenovic, J. Brivio, V. Giacometti, and A. Kis, Nat. Nanotechnol. **6**, 147 (2011).
[4] K. F. Mak, C. Lee, J. Hone, J. Shan, and T. F. Heinz, Phys. Rev. Lett. **105**, 136805 (2010).
[5] D. Xiao, G.-B. Liu, W. Feng, X. Xu, and W. Yao, Phys. Rev. Lett. **108**, 196802 (2012).
[6] H. Zeng, J. Dai, W. Yao, D. Xiao, and X. Cui, Nat. Nanotechnol. **7**, 490 (2012).
[7] K. F. Mak, K. He, J. Shan, and T. F. Heinz, Nat. Nanotechnol. **7**, 494 (2012).
[8] S. A. Wolf, D. D. Awschalom, R. A. Buhrman, J. M. Daughton, S. von Molnár, M. L. Roukes, A. Y. Chtchelkanova, and D. M. Treger, Science **294**, 1488 (2001).
[9] W. S. Yun, S. W. Han, S. C. Hong, I. G. Kim, and J. D. Lee, Phys. Rev. B **85**, 033305 (2012).
[10] K. Chang and W. Chen, ACS Nano **5**, 4720 (2011).
[11] Y. Li, H. Wang, L. Xie, Y. Liang, G. Hong, and H. Dai, J. Am. Chem. Soc. **133**, 7296 (2011).
[12] S. Murakami, Phys. Rev. Lett. **97**, 236805 (2006).
[13] M. Wada, S. Murakami, F. Freimuth, and G. Bihlmayer, Phys. Rev. B **83**, 121310(R) (2011).
[14] Z. Liu, C.-X. Liu, Y.-S. Wu, W.-H. Duan, F. Liu, and J. Wu, Phys. Rev. Lett. **107**, 136805 (2011).
[15] T. Hirahara, G. Bihlmayer, Y. Sakamoto, M. Yamada, H. Miyazaki, S. I. Kimura, S. Blügel, and S. Hasegawa, Phys. Rev. Lett. **107**, 166801 (2011).
[16] F. Yang, L. Miao, Z. F. Wang, M.-Y. Yao, F. Zhu, Y. R. Song, M.-X. Wang, J.-P. Xu, A. V. Fedorov, Z. Sun, G. B. Zhang, C. Liu, F. Liu, D. Qian, C. L. Gao, and J.-F. Jia, Phys. Rev. Lett. **109**, 016801 (2012).
[17] E. I. Rashba, Fiz. Tverd. Tela **2**, 1224 (1960) [Sov. Phys. Solid State **2**, 1109 (1960)].
[18] S. Datta and B. Das, Appl. Phys. Lett. **56**, 665 (1990).
[19] S. LaShell, B. A. McDougall, and E. Jensen, Phys. Rev. Lett. **77**, 3419 (1996).
[20] M. Hoesch, M. Muntwiler, V. N. Petrov, M. Hengsberger, L. Patthey, M. Shi, M. Falub, T. Greber, and J. Osterwalder, Phys. Rev. B **69**, 241401(R) (2004).

[21] A. Varykhalov, D. Marchenko, M. R. Scholz, E. D. L. Rienks, T. K. Kim, G. Bihlmayer, J. Sánchez-Barriga, and O. Rader, Phys. Rev. Lett. **108**, 066804 (2012).
[22] C. R. Ast, J. Henk, A. Ernst, L. Moreschini, M. C. Falub, D. Pacilé, P. Bruno, K. Kern, and M. Grioni, Phys. Rev. Lett. **98**, 186807 (2007).
[23] O. Krupin, G. Bihlmayer, K. Starke, S. Gorovikov, J. E. Prieto, K. Döbrich, S. Blügel, and G. Kaindl, Phys. Rev. B **71**, 201403(R) (2005).
[24] Yu. S. Dedkov, M. Fonin, U. Rüdiger, and C. Laubschat, Phys. Rev. Lett. **100**, 107602 (2008).
[25] P. E. Blöchl, Phys. Rev. B **50**, 17953 (1994).
[26] G. Kresse and D. Joubert, Phys. Rev. B **59**, 1758 (1999).
[27] G. Kresse and J. Furthmüller, Phys. Rev. B **54**, 11169 (1996).
[28] J. P. Perdew, K. Burke, and M. Ernzerhof, Phys. Rev. Lett. **77**, 3865 (1996).
[29] J. Klimes, D. R. Bowler, and A. Michaelides, J. Phys. Condens. Matter **22**, 022201 (2010).
[30] P. V. C. Medeiros, S. Stafström, and J. Björk, Phys. Rev. B **89**, 041407(R) (2014); P. V. C. Medeiros, S. S. Tsirkin, S. Stafström, and Jonas Björk, *ibid.* **91**, 041116(R) (2015).
[31] V. Popescu and A. Zunger, Phys. Rev. B **85**, 085201 (2012).
[32] For instance, the corresponding spin components are not polarized at the *K* point because it is the Zeeman splitting that occurs there.
[33] A. Varykhalov, J. Sánchez-Barriga, A. M. Shikin, W. Gudat, W. Eberhardt, and O. Rader, Phys. Rev. Lett. **101**, 256601 (2008).
[34] S. M. Huang, A. O. Badrutdinov, L. Serra, T. Kodera, T. Nakaoka, N. Kumagai, Y. Arakawa, D. A. Tayurskii, K. Kono, and K. Ono, Phys. Rev. B **84**, 085325 (2011).
[35] J. Nitta, T. Akazaki, H. Takayanagi, and T. Enoki, Phys. Rev. Lett. **78**, 1335 (1997).
[36] K. Ishizaka, M. S. Bahramy, H. Murakawa, M. Sakano, T. Shimojima, T. Sonobe, K. Koizumi, S. Shin, H. Miyahara, A. Kimura, K. Miyamoto, T. Okuda, H. Namatame, M. Taniguchi, R. Arita, N. Nagaosa, K. Kobayashi, Y. Murakami, R. Kumai, Y. Kaneko, Y. Onose, and Y. Tokura, Nat. Mater. **10**, 521 (2011).
[37] J. Park, S. W. Jung, M.-C. Jung, H. Yamane, N. Kosugi, and H. W. Yeom, Phys. Rev. Lett. **110**, 036801 (2013).